VILNIUS TECH
Vilnius Gediminas Technical University

Journal of Environmental Engineering and Landscape Management
ISSN 1648–6897 / eISSN 1822-4199
2022 Volume 30 Issue 1: 66–80
https://doi.org/10.3846/jeelm.2022.16286

COMBINED ACTION OF ADSORPTION AND CATALYTIC OXIDATION IN ALUMINUM DYE REMOVAL BY GROUNDWATER TREATMENT WASTE

Edita SODAITIENĖ, Danutė KAUŠPĖDIENĖ, Audronė GEFENIENĖ*, Romas RAGAUSKAS, Rimantas RAMANAUSKAS

Center for Physical Sciences and Technology, Saulėtekio al. 3, LT-10257 Vilnius, Lithuania

Received 22 April 2021; accepted 17 August 2021

Highlights

- The groundwater treatment sludge (GWTW) is an effective, cheap, and environmentally friendly Fenton-like heterogeneous catalyst.
- GWTW promotes the degradation of an anodized aluminum dye.
- The solution decoloration rate increased with the decrease in pH and increase in temperature.

Abstract. The performance of groundwater treatment waste (GWTW) as an adsorbent and catalyst in the decoloration of aluminum dye Sanodure green LWN (SG) solution was investigated. The raw GWTW was more suitable for dye removal than calcined at 800 °C temperature. The catalytic activity of GWTW in Fenton-like reactions in sunlight increases with decreasing pH from 5.5 to 2.5 and increasing temperature from 20 to 60 °C. The rate of 70% decoloration in the first 5 min and 92% after 50 min of 100 mg/L SG dye solution was reached at 50 °C and pH 3. Kinetics of the SG dye color removal fitted well with the double exponential and two-stage pseudo-first-order kinetic models. The activation energy of the first stage of the SG dye degradation reaction is 30.45 kJ/mol. GWTW could be re-used for the pre-treatment of dye-contaminated wastewater before entering the wastewater treatment plant.

Keywords: waste management technologies, groundwater treatment waste, adsorption, heterogeneous catalysis, dye removal.

Introduction

From ancient times, the people desired to look at colorful, beautiful-looking products in their environment and used them extensively in daily life. Unfortunately, the chemical compounds that give the color can be harmful to the environment and dangerous for humans (Mittal, 2020). It is well known that large quantities of organic dyes are consumed in the textile industry. However, metal coloring is also performed both for technical and decorative purposes. Surfaces of aluminum alloys are usually protected by forming anodic films that can be colored (Chang et al., 2016). The color range of anodized aluminum depends not only on the aluminum alloy base but also on the dye composition. Mono-azo, poly-azo, and metal complex organic dyes are widely used for aluminum coloring. Therefore, they fall into the wastewater. Metal complex dyes contain not only complex aromatic ligands but also heavy metals, which increase their toxicity (Sanodure Green Safety datasheet, 2020; Hou et al., 2016). Such wastewater needs to be purified, so that clean water is returned to production.

Although colored anodized aluminum is often used in various decorative products, nowadays, wastewater contaminated with dyes is usually treated according to the dye removal technology traditionally applied in the textile industry. However, metals and textiles are dyed differently, which is one of the factors determining the wastewater treatment processes (Chang et al., 2016; Banazadeh et al., 2016).

Adsorption has become one of the most frequently used technologies for the removal of dyes. Polymeric biocomposites (Noreen et al., 2020), biomass and its magnetic composites (Jabeen & Bhatti, 2021), chitosan-based adsorbents (Kausar et al., 2021) have been tested for dye adsorption. Waste materials and products of their modification were also utilized as adsorbents to remove organic

*Corresponding author. E-mail: *audrone.gefeniene@ftmc.lt*

dyes (Mittal & Mittal, 2015); Haddad et al., 2021). Efficient removal of various dyes (Malachite Green, Crystal Violet, Rhodamine B, Methylene Blue, Chrysoidine R, and Congo Red) was attained using carbon-based materials as adsorbents: activated carbon (Arora et al., 2020; Patel et al., 2021), metal-organic framework (Soni et al., 2020), carbon nanofibers (Saharan et al., 2021), ordered mesoporous carbon (Mariyam et al., 2021a, 2021b) and activated carbon nanocomposite (Gupta et al., 2020). A novel surface imprinted resin with selective adsorption capability and the dye recognition ability was synthesized and showed excellent adsorption performance (Sun et al., 2021). An innovative adsorbent coating technology for industrial wastewater treatment is extensively studied (Azha et al., 2021).

The advanced oxidation processes (AOPs) are widely applied for the decomposition of various organic contaminants (Bhat & Gogate, 2021; Banazadeh et al., 2016; Horáková et al., 2014; Oller et al., 2011). Using AOPs and nanostructured metals or metal oxides as catalysts, the hydroxyl radicals (•OH) from H_2O_2 are generated, which break down organic pollutants into CO_2, H_2O, and small organic molecules (Neyens & Baeyens, 2003). The elements of varying oxidation states such as iron, manganese, copper, chromium, cobalt, cerium, and ruthenium can activate hydrogen peroxide (H_2O_2) in both homogeneous and heterogeneous reactions under neutral or alkaline conditions (Bokare & Choi, 2014).

Iron-based nanoparticles of various types are materials of interest in the role of catalysts or adsorbents in water and wastewater treatment (Aragaw et al., 2021).

Iron oxides, hydroxides, and oxyhydroxides are classified as promising heterogeneous Fenton catalysts (Thomas et al., 2021; Garrido-Ramírez et al., 2010). Natural iron minerals and synthetic iron materials are widely used to treat organic contaminants (Luo et al., 2021). The main positive features are their abundance, negligible toxicity, low cost, and high catalytic activity (Thomas et al., 2021). The advantage of heterogeneous catalysts is that they are active in acidic and near-neutral media (Moradi et al., 2020). The catalytic efficiency of heterogeneous Fenton catalysts depends on their physical and chemical properties, structural and surface characteristics (Domacena et al., 2020; Garrido-Ramírez et al., 2010). In a heterogeneous Fenton system, the reduction of Fe(III) to Fe(II) by H_2O_2 is the degradation speed limiting step (Lai et al., 2021). Heterogeneous Fenton reactions can be accelerated using novel strategies: promoting H_2O_2 decomposition, controlling catalyst morphology, or introducing electron-rich materials (Zhu et al., 2019). The efficiency of the heterogeneous Fenton process was improved by using the nanomaterial composed of ferric oxide, silica, and alumina (Nguyen et al., 2021). Degradation of Synozol Red reactive dye was achieved using $ZnFe_2O_4$ catalyst and the composite prepared from $ZnFe_2O_4$ and graphene oxide (Nadeem et al., 2020). Nanocomposites of goethite and akaganeite demonstrated photocatalytic activity by removing the color of Methyl Orange (Pal et al., 2020). Iron compounds can be supported on other solid materials (Thomas et al., 2021; Garrido-Ramírez et al., 2010). Iron-containing catalysts loaded on activated carbon (Rubeena et al., 2018) or silica (Perrotti et al., 2019) enhanced the dye degradation.

Very often, homogeneous and heterogeneous Fenton reactions occur simultaneously, especially in acidic mediums. The iron leached from the solid surface may initiate a homogeneous process (Thomas et al., 2021), and therefore, various iron-rich materials demonstrate stronger catalytic activity (Li et al., 2020). The contribution of heterogeneous and homogeneous processes was studied by Prucek and coworkers (Prucek et al., 2009). The role of homogeneous reaction in the generation of •OH radicals was considered using α-FeOOH as a catalyst (Miao et al., 2018).

The synergistic effect of adsorption and the Fenton process using bifunctional materials is widely explored (Bello & Raman, 2019). Adsorption and catalysis using activated carbons and H_2O_2 were combined for the decoloration of dye solutions (Santos et al., 2009). The impact of adsorption and catalytic activation on removing of Methyl Orange dye by iron oxyhydroxides supported on amino-functionalized silica was determined (Perrotti et al., 2019).

Recently, the catalytic activity of wastes of various compositions generated during industrial processes has been tested. These iron-rich solids may be suitable for activating hydrogen peroxide. Using steel-making or goldmine waste as catalysts instead of iron salts can reduce the cost of treating wastewater contaminated with methyl orange and other dyes without compromising process efficiency (Ali et al., 2013; Montoya-Bautista et al., 2019; Huang et al., 2011). FeO-containing iron slag wastes were employed to degrade Reactive Red 24 dye in an aqueous solution (Van et al., 2019). Amorphous FeOOH was prepared from fly ash and used as a heterogeneous photo-Fenton catalyst (Li & Zhang, 2010). The deposits formed on the internal surfaces of pipes from the drinking water network usually are rich in various forms of iron oxyhydroxides. The possibility of catalytic degradation of the pesticide paraquat with hydrogen peroxide and the real pipe deposits as catalysts was studied (Oliveira et al., 2012). Ferric waste sludge produced during the purification of water was employed for the catalytic oxidation of volatile organic compounds (VOCs) with H_2O_2 (Sanchis et al., 2019).

In this study, the groundwater treatment waste (GWTW) and H_2O_2 were used as environmentally friendly materials in the roles of an adsorbent/catalyst and an oxidant, respectively. We explored sunlight as a cheap and sustainable source of energy.

The groundwater treatment waste (GWTW) is formed by removing iron and manganese from groundwater by aeration (Zubrytė et al., 2020). Nowadays, the reuse of drinking water treatment sludge has become an increasingly important issue (Babatunde & Zhao, 2007). Therefore, GWTW is extensively studied as a suitable adsorbent for nickel, cadmium, and CO_2 (Wołowiec et al., 2019; Ong et al., 2017; Siswoyo et al., 2014; Novoselova, 2013) and as a coagulant to remove natural organics from river water (Albrektienė et al., 2019).

Since Fe_2O_3 predominates in the groundwater treatment waste (GWTW), it could be a cheap and easily accessible adsorbent/Fenton-like catalyst for the removal of dyes. In the literature, we have not yet been able to find the results of such studies. Therefore, the purpose of our work was to assess the performance of GWTW as natural bifunctional material in the decoloration of the anodized aluminum dye Sanodure Green LWN (SG) solution. The choice of low-cost, efficient, and environmentally friendly catalysts is particularly relevant for small businesses involved in the small-scale production of colored aluminum parts. The synergetic effect of GWTW and H_2O_2 in the adsorption and oxidation of the dye was evaluated under different solution pH and temperature conditions. The SG dye removal experiments in the absence of H_2O_2 or GWTW were also carried out to assess the advantage of the combined process of adsorption and catalytic oxidation.

1. Materials and methods

Groundwater treatment waste (GWTW) was obtained from the Antaviliai drinking water supply station in Vilnius, Lithuania. Raw GWTW was air-dried in the laboratory at room temperature for 4 weeks. After that, it was finely crushed in a pestle and stored in a desiccator. Before X-ray diffraction analysis and the experiments with calcined GWTW, the samples were preheated at 800 °C in a muffle furnace for 5 h in an air atmosphere.

Commercial adsorbents, including activated carbon NORIT PK 1–3 (Cabot Norit), macroporous resins (weak base Macronet MN 150, non-ionic Macronet MN 200, strong acid Macronet MN 500 (Purolite Company)), and mixed bed resin PMB 101 (Pure Resin Co., Ltd) were used to compare their adsorption capacity for SG dye.

The Sanodure Green LWN (SG) dye for anodized aluminum was obtained from Clariant International Ltd. Switzerland. It belongs to the azo dyestuff/chromium complex anionic dye family (Figure 1).

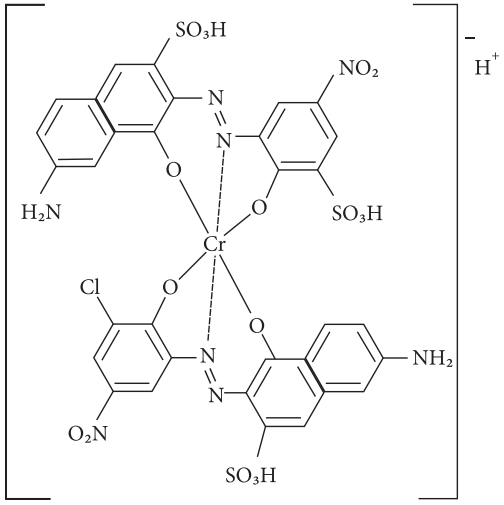

Figure 1. Structure of the chromium complex anionic dye suitable for anodized aluminum dyeing (Heber, 2015)

A scanning electron microscope EVO 50EP (Carl Zeiss SMT AG) with a secondary electron detector (low vacuum mode, 10 kV, 50 Pa, working distance 10 mm) was used to investigate of GWTW surface morphology.

FTIR spectra of GWTW and SG dye were recorded from 100 scans in the range of 650–4000 cm^{-1} by spectrometer ALPHA (Bruker, Germany).

X-ray powder diffraction (XRD) data for the preheated GWTW were obtained with an X-ray diffractometer SmartLab (Rigaku, Japan), equipped with a 9 kW rotating Cu anode X-ray tube. The measurements were done in the range $2\theta = 15–60°$. Phases of GWTW were identified using the software package PDXL (Rigaku) and ICDD powder diffraction database PDF-4+ (2013). X-ray fluorescence spectrometer AxiosmAX (PANalytical, Netherlands) with wave dispersion (XRF-WD) and 4 kW Rh anode was used to ascertain the elemental composition of dry GWTW specimens. For testing, the samples were primed up to micron particle size (rotary mill 550 rpm for 5 min), and 37 mm diameter tablets were compressed by a hydraulic press at 150 KN cm^{-2}. Omnian (PANalytical) software was applied for the quantification of elements in the standardless analysis. Chemical composition was adjusted using benchmarks ESK, IMZ-267, PI 3.13, NCSDC18013, and NCSD60105. XPS analysis was performed using ESCALAB MKII spectrometer fitted with an XR4 twin anode.

The combined adsorption and catalytic degradation experiments were conducted as follows: into a 10 mL of aqueous SG dye solution (100 mg/L) at a temperature of 20 °C, 50 °C, or 60 °C 5 mg of GWTW was poured. After that pH of the system was adjusted with 5 M HCl, and the pre-determined optimal amount of 1 mL of hydrogen peroxide H_2O_2 (35 wt.%) was immediately added. During the reaction time, the mixture was constantly stirred. The solution color faded when the reaction proceeded. After some scheduled time, 5 ml of centrifuged supernatant was carefully transferred into a quartz cuvette for UV-visible spectral measurement. After that, the solution and sludge were transferred back to the adsorption/catalytic reaction vessel. The procedure was repeated to follow the dye removal progress, and UV-visible spectra were recorded at the pre-determined time. For comparison, at the same conditions, adsorption tests were performed with GWTW and without H_2O_2 or non-catalytic oxidation with H_2O_2 and without a solid phase. A series of catalytic experiments were also conducted with an introductory adsorption step during which the flasks with SG dye solutions and GWTW were stirred for 30 min in the dark without the addition of H_2O_2 (Xiao et al., 2018).

The degradation rate of the SG dye (color removal efficiency, RE) was assessed by measuring UV-visible spectra with a Varian Cary 50 spectrometer (Agilent Technologies, USA). Based on the UV-vis absorbance data at the wavelength of 630 nm, the removal efficiency was calculated according to Eq. (1):

$$\text{Removal efficiency, \%} = \frac{(A_0 - A_t)}{A_0} \times 100\ \%\,, \qquad (1)$$

where A_0 is the dye solution absorbance at $t = 0$; A_t is the absorbance at a time t.

The sorption capacity of the GWTW q (mg/g) was calculated according to Eq. (2):

$$q, \text{ mg/g} = \frac{(C_0 - C_t) \times V}{m}, \quad (2)$$

where C_0 and C_t are the concentrations (mg/L) of the SG dye in the solution before and after sorption determined from the calibration curve $A = f(C)$, respectively. V is the volume of the dye solution (L), and m is the dry GWTW (g) mass.

2. Results and discussion

2.1. Characterization of the GWTW

The scanning electron microscopy image of the raw GWTW dried at room temperature is shown in Figure 2a. It shows that the powder consists of 50–200 nm spherical particles adhering to each other into agglomerates.

Groundwater supplied to Lithuanian consumers is of calcium-magnesium-bicarbonate type (Diliūnas et al., 2006). X-ray diffraction analysis of raw GWTW has shown that this material at room temperature was of amorphous character. The chemical composition and physical properties of iron(III) hydroxide differ from the initial state before heating (Kan et al., 2016). From the X-ray diffractogram presented in Figure 2b, we can conclude a crystalline cubic phase of maghemite (γ-Fe_2O_3; ICDD 00–039-1346) and hexagonal phase of SiO_2 (ICCD 00–046-1045) was formed after the heating of a GWTW sample at 800 °C in an air atmosphere. The presence of SiO_2 in GWTW is a result of a groundwater flow through a sand filter. The X-ray fluorescence spectroscopy confirmed that the GWTW is eco-friendly material rich in iron compounds. In the air-dried sediment, the percentage of iron and oxygen was 43.5 wt% and 44.9 wt%, respectively. The composition of GWTW expressed in the form of oxides is as follows: 77.99% Fe_2O_3, 5.23% SiO_2, 7.37% CaO, 7.42% P_2O_5, 0.48% MnO, 0.57% SO_3, and 0.32% MgO. The data of X-ray fluorescence spectroscopy showed that the content of Al, Ba, Sr, K, Ti, As, and Cl do not exceed 0.1 wt%. The detected chemical elements are transferred to GWTW from the groundwater in the form of insoluble compounds together with iron hydroxides and oxides.

The chemical state of Fe and O elements in raw GWTW was determined by XPS analysis (Figure 3). In the Fe 2p spectrum, Fe $2p_{1/2}$ peak at 725 eV and Fe $2p_{3/2}$ peak at 712.3 eV can be related to the Fe-OH binding energy in the hydrous ferric oxides and oxyhydroxides (goethite, lepidocrocite). Meanwhile, the Fe $2p_{3/2}$ peak at 710.5 eV corresponds to the Fe-O binding energy in hematite (α-Fe_2O_3) (McIntyre & Zetaruk, 1977; Grosvenor et al., 2004). In the O 1s spectrum, peaks at 529.5 eV, 530.54 eV, 531.6 eV correspond to oxygen binding with Fe (Fe-O) and hydroxyl binding with Fe (Fe-OH). The peak at 532.9 eV can be assigned to molecular water (McIntyre & Zetaruk, 1977; Grosvenor et al., 2004; Leiviskä et al., 2019). As the major components of GWTW are hydrous ferric oxides ($Fe_2O_3 \cdot nH_2O$), iron oxyhydroxides (FeOOH), and oxides (Fe_2O_3), it can activate the decomposition of hydrogen peroxide to its radicals.

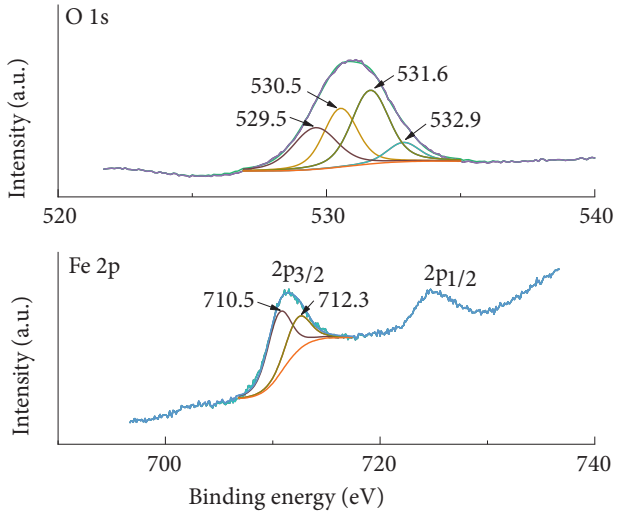

Figure 3. The high-resolution XPS spectra of O 1s and Fe 2p of raw GWTW

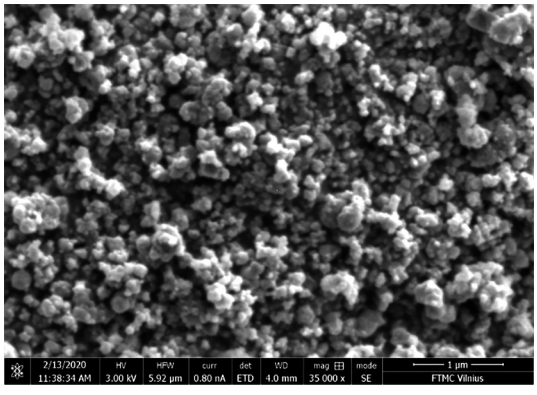

a)

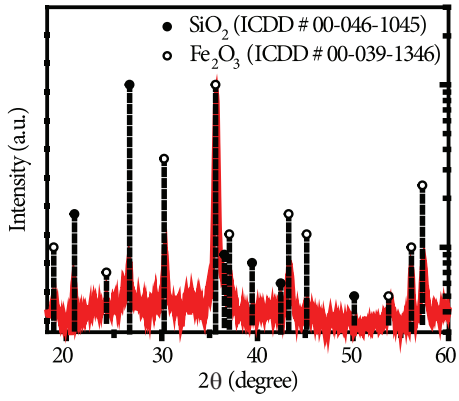

b)

Figure 2. SEM image of the raw GWTW dried at room temperature (a) and XRD spectrum of the GWTW surface after 5 h heating at 800 °C in an air atmosphere (b)

The adsorption capacity and catalytic activity are strongly related to the specific surface area of iron-oxide minerals (Garrido-Ramírez et al., 2010). The BET-specific surface area of raw GWTW dried at room temperature and used in this work for the SG dye adsorption and destruction was 34.76 $m^2\ g^{-1}$ (Sodaitienė et al., 2021).

FTIR analysis of GWTW and SG dye was carried out to identify the functional groups and chemical bonds. The FTIR spectra are presented in Figure 4.

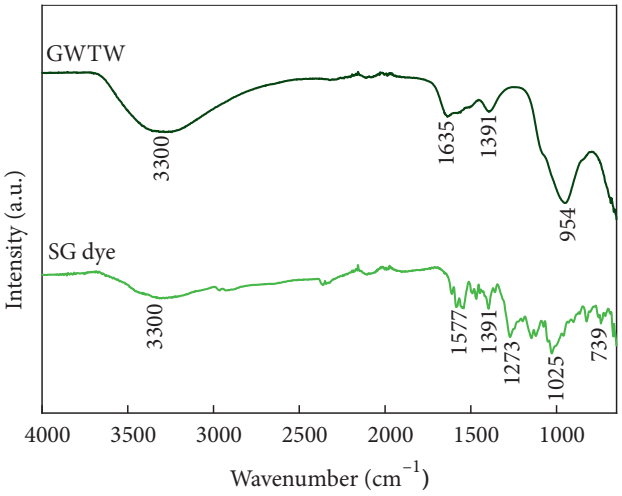

Figure 4. FTIR spectra of metal-complex SG dye and groundwater treatment waste

FTIR spectrum of SG dye shows peaks characteristic to azo dyes (Prati et al., 2016). The peaks located at 1472 cm^{-1} can be ascribed to azo bond (N = N) vibrations (Prati et al., 2016). The peaks between 1000 and 1200 correspond to the SO_3 group: symmetric stretching vibrations of S = O bonds at 1025 cm^{-1} and 1121 cm^{-1} (Sun et al., 2021) and asymmetric vibrations at 1147 cm^{-1}. The peaks in the region of 1391 cm^{-1} can be attributed to the symmetrical and asymmetrical bending vibrations of the CH_3 functional groups (Bartošová et al., 2017). The peak located at 1273 cm^{-1} can be ascribed to the C-N aromatic stretching vibrations (Katsoukis et al., 2019). The peaks observed at 1541 cm^{-1}, 1577 cm^{-1}, and 1610 cm^{-1} are assigned to the aromatic C = C vibrations of the dye (Prati et al., 2016). The spectrum exhibits the out-of-plane C-H bending vibrations of aromatic rings at 825 cm^{-1} and 739 cm^{-1} (Paredes-Laverde et al., 2021). The broad band in the region of 3000–3600 cm^{-1} can be attributed to the stretching vibrations of O-H and N-H (Prati et al., 2016).

The broad band at 3000–3600 cm^{-1} is characteristic of the stretching vibrations of O-H bonds in adsorbed water molecules. The peak located at 1635 cm^{-1} corresponds to the bending vibration of O-H of adsorbed water (Tang et al., 2019). The peak at 1391 cm^{-1} shows the C-O bonds in the adsorbed carbonates (Ociński et al., 2016). Bending vibration of Fe-O bonds is observed at 954 cm^{-1}. A band in the region of 670 cm^{-1} comes from the Fe-O stretching vibration (Zhang et al., 2017).

2.2. Decoloration of SG dye solutions using three different approaches

The SG dye removal experiments have been carried out using three different approaches to elucidate the catalytic activity of GWTW in a Fenton-like reaction. The solution decoloration efficiency using the catalytic degradation approach was evaluated for the systems containing GWTW as a potential catalyst and hydrogen peroxide as an oxidant. For comparison, a simple adsorption process without the presence of H_2O_2 was applied for the removal of color under the same experimental conditions (pH, temperature, solution volume to GWTW mass ratio). The analogous control tests were also performed to ascertain the ability of H_2O_2 alone to degrade the SG dye molecules. The process of SG dye solution decoloration was monitored by UV-visible spectral measurements (Figure 5). The pathway of SG dye oxidation with H_2O_2 in the presence of GWTW can be considered by examining the UV-vis spectra presented in Figure 5a. The immediate

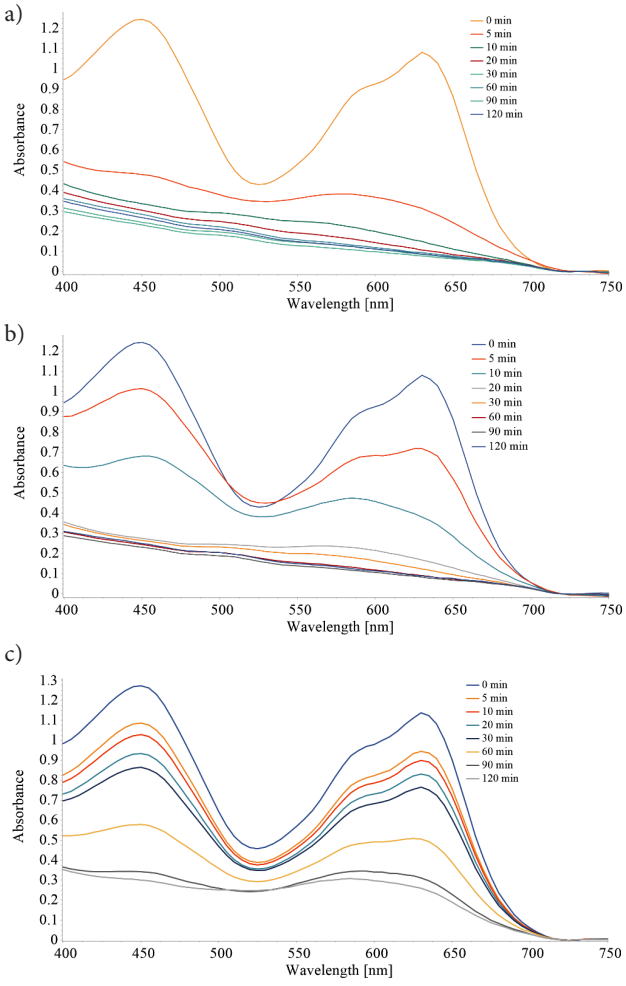

Figure 5. Time-dependent absorption spectra of the SG dye solution before and during: (a) degradation reaction with H_2O_2 and GWTW catalyst; (b) adsorption on GWTW in the absence of H_2O_2; (c) non-catalytic degradation with H_2O_2 in the absence of GWTW. Conditions: concentration of SG dye 100 mg/L, volume of dye solution 10 mL, 5 mg GWTW, 1 mL H_2O_2, pH 3, T = 50 °C

fast decoloration of SG dye solution was observed at the beginning of the catalytic reaction.

More than 70% decoloration was achieved during the first 5 min, and the main peaks disappeared after 10 min of the reaction. In comparison, 32% and 63% decoloration was attained in the SG dye adsorption process after the same periods of time (Figure 5b). In the case of non-catalytic peroxidation of the SG dye molecules, both characteristic peaks gradually decreased over the reaction time during the degradation reaction (Figure 5c). By comparing the spectra presented in Figure 5a-c, it is clear that the addition of H_2O_2 to the system containing GWTW improved the SG dye removal process. The combination of GWTW as adsorbent and heterogeneous catalyst with H_2O_2 as oxidant reveals the synergistic effect and the increased potential of the used solid amorphous material in the removal of SG dye. As can be observed from Figure 5c, the peroxidation without the presence of GWTW was the least effective, and the absorbance of the SG dye solution decreased slowly and gradually. In this case, the color intensity of the SG dye solution was lost because of the direct attack of H_2O_2 on SG dye molecules (Santos et al., 2009).

As we can see from the photograph in Figure 6, the visual appearance of GWTW during the Fenton-like catalytic degradation of the dye differs from that in the case of the SG dye adsorption without the addition of the H_2O_2 oxidant. When the catalytic degradation proceeds, the GWTW particles regain their original color. In contrast, the GWTW surface acquires the dark green color after the coverage with SG dye molecules during the adsorption process. It is evident that the removal of the SG dye using the catalytic oxidation approach leads to the destruction of the dye molecule structure. Our future investigations aim is to determine the COD and TOC parameters for the SG dye solution before and after the treatment with GWTW and H_2O_2. It is essential to ascertain the ability of GWTW to adsorb the dye degradation products, including chromium. As it was mentioned earlier, the specific surface area of the GWTW measured by the BET method was relatively large, up to 35 $m^2\ g^{-1}$. The value of this parameter significantly affects the pollutant removal efficiency by applying adsorption as a single independent method. However, the BET surface area of the material also determines its catalytic performance because the degradation process is related to the adsorption of pollutants and oxidizing agents on the surface of the catalyst. A higher number of active centers can be expected in a larger specific surface area of heterogenous catalyst (Zheng et al., 2015).

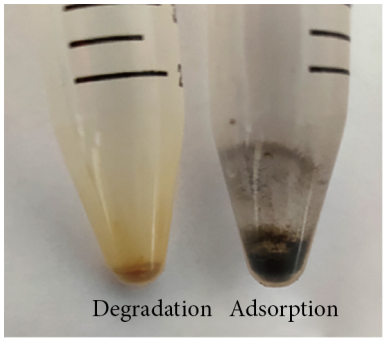

Figure 6. A photograph of the GWTW: (in the left) in the case of the catalytic degradation of SG dye with H_2O_2; (in the right) in the case of the adsorption of SG dye without H_2O_2

The improved action of GWTW in the presence of H_2O_2 can be seen from the kinetic curves of SG dye removal (Figure 7). It is obvious that the higher color removal rate may be achieved by the combined process of adsorption and catalytic degradation rather than by adsorption alone. By comparing the curves presented in Figure 7, we can see that the addition of H_2O_2 to the system containing GWTW accelerated the SG dye removal process. The processes of combined adsorption/Fenton-like oxidation (degradation), adsorption alone, and non-catalytic oxidation with H_2O_2 (peroxidation) were modeled by a double exponential model (Guz et al., 2014). Experimental data for the three different systems were fitted with a double exponential equation:

$$\frac{C}{C_0} = a \times e^{-k_1 t} + b \times e^{-k_2 t}, \tag{3}$$

where C is the SG dye concentration at time t, C_0 – initial concentration; k_1 and k_2 – reaction rate constants.

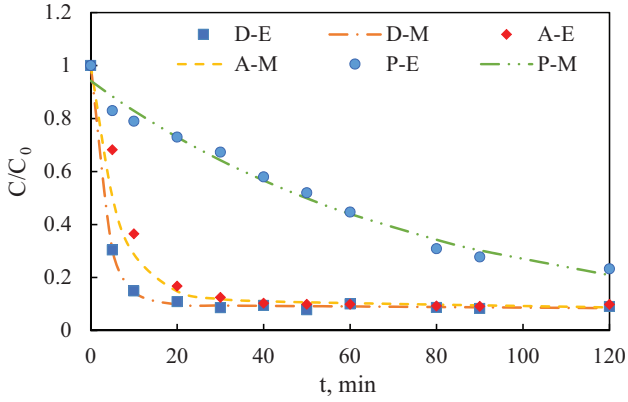

Figure 7. Experimental (E) kinetic data (symbols) and double exponential model (M) fits (lines) for the SG dye removal in different systems: SG+GWTW+H_2O_2 (Degradation (D)), SG+GWTW (Adsorption (A)), SG+H_2O_2 (Peroxidation (P)). Conditions: concentration of SG dye 100 mg/L, volume of dye solution 10 mL, 5 mg GWTW, 1 mL H_2O_2, pH 3, T = 50 °C

As we can see from Figure 7, the experimental data fit well in the double exponential model with the R^2 values >0.98. Correlation coefficients and the kinetic parameters data are presented in Table 1. The dye removal rate constants listed in Table 1 showed that $k_1 > k_2$ for all the examined processes except for homogeneous peroxidation at 20 °C. In the case of non-catalytic peroxidation, initial color removal rate constants k_1 are relatively low, especially at 20 °C temperature (Table 1).

Table 1. Kinetic parameters based on the double exponential model for the removal of SG dye using degradation, adsorption, and peroxidation approaches

System	R^2	a	k_1 (min^{-1})	b	k_2 (min^{-1})
SG+GWTW+H_2O_2 Degradation 20 °C	0.9958	0.7603	0.3175	0.2384	0.0076
SG+GWTW Adsorption 20 °C	0.9981	0.7209	0.2620	0.2777	0.0066
SG+H_2O_2 Peroxidation 20 °C	0.9980	0.8491	0.0026	0.1507	0.3979
SG+GWTW+H_2O_2 Degradation 50 °C	0.9993	0.9020	0.2926	0.0977	0.0012
SG+GWTW Adsorption 50 °C	0.9988	0.8781	0.1650	0.1222	0.0028
SG+H_2O_2 Peroxidation 50 °C	0.9811	0.8351	0.0135	0.1075	0.0075

2.3. pH effect on SG dye degradation efficiency

The effect of solution pH on the systems of combined adsorption and heterogeneous catalysis was studied at a pH range of 2.0–5.5 (acidic and slightly acidic conditions). The importance of solution pH for the SG dye removal efficiency can be seen in Figure 8. It shows the results of the SG dye removal study performed involving an initial step called pre-adsorption. During this pre-adsorption period, the color intensity of the SG dye solution decreased due to the interaction of SG dye with GWTW in the dark in the absence of H_2O_2. The data presented in Figure 8 show that the SG dye uptake by adsorption in the dark during the first 30 min is highly dependent on the solution pH. The dye removal efficiency (RE) increases from 16.8 to 51% as the pH of the solution decreases from 3.3 to 2.0. This is because the adsorption capacity of GWTW changes from 28.9 mg/g to 95.5 mg/g after acidification of the solution from pH 3.3 to pH 2.0. When the pH of the dye solution was not adjusted before the addition of H_2O_2 (pH_0 5.0), the adsorption of SG dye molecules was very negligible (Figure 8). However, the color fading was initiated when the H_2O_2 oxidant entered the adsorption system, and up to 30% of the dye was removed within 120 min. As we can see from Figure 8, the acidic medium (pH 2.0–3.3) is more favorable for the dye's adsorption and for oxidative dye molecule degradation. In the presence of H_2O_2, the rate of decoloration increases with decreasing pH. At pH 2.0, the high removal efficiency of 73% can be achieved as early as 5 min after the start of the reaction (Figure 8).

The results of tests of combined adsorption and heterogeneous catalysis carried out without the initial stage of simple adsorption are presented in Figure 9. The dye removal progress demonstrates a similar trend, and the decoloration of the SG dye solution was more efficient in a more acidic medium (Figure 9). The color removal was very fast during the first 5 min when the solution pH was in the range of pH 2.0–2.5. Decoloration degree was lower in the system with pH 3.7, but it gradually increased with time. At the same time the

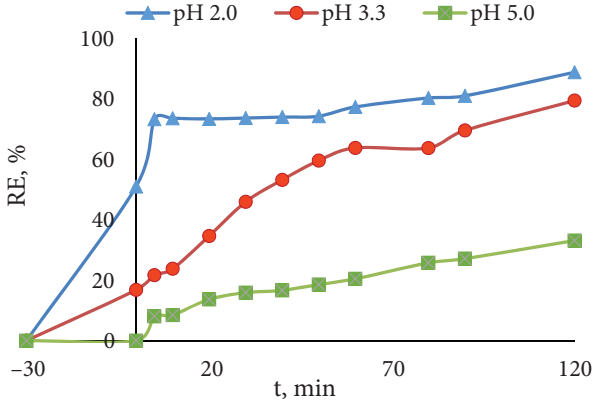

Figure 8. Effect of pH on the SG dye removal during the two-stage process: the first stage (–30 min–0 min) – adsorption in the dark, the second stage (0 min–120 min) – combined adsorption/catalytic oxidation. Conditions: SG dye solution concentration 100 mg/L, dye solution volume 10 mL, 1 mL H_2O_2, 5 mg GWTW catalyst, T 20 °C

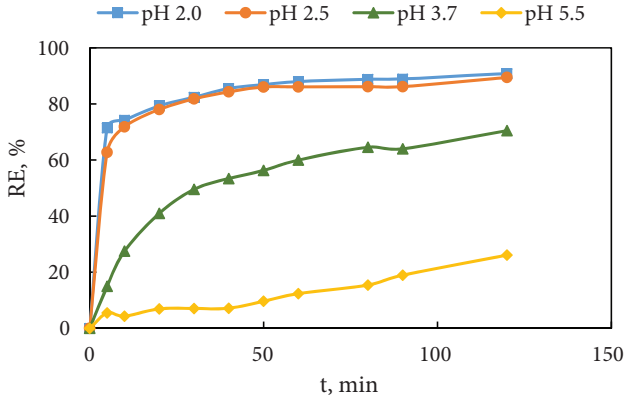

Figure 9. Effect of pH on the SG dye removal by combined adsorption/catalytic oxidation. Conditions: concentration of SG dye 100 mg/L, the volume of dye solution 10 mL, 1 mL H_2O_2, 5 mg GWTW catalyst, T 20 °C

dye removal efficiency was rather low in slightly acidic conditions (pH 5–6).

The better performance of the process around pH 2–3 could be explained by the chemical properties and composition of the used solid material. The point of zero charge (pH_{pzc}) of GWTW is equal to pH = 8.0 (Zubrytė et al., 2020), thus under experimental conditions used, the GWTW surface was positively charged (Dzombak & Morel, 1990). In the acidic medium, the protonation of GWTW increased, which means that the adsorption occurred according to the mechanism of the electrostatic interaction between the positively charged GWTW surface and the dye anion. Additionally, the pH affects the •OH radical formation rate (Yao et al., 2013; Rubeena et al., 2018). A homogeneous Fenton reaction can also be expected in the acidic medium. As has already been determined in our previous work (Zubrytė et al., 2020), the concentration of Fe(III) in the solution with pH 2 was about 120 mg/L. Similar results were obtained for burger-like Fe_2O_3 (Xiao et al., 2018), where the optimal pH range for the degradation of Acid Red G dye was determined about 2–3. Homogeneous non-catalytic peroxidation of SG dye was also dependent on solution pH (data not shown).

2.4. Effect of dose of the catalyst

The activity of GWTW catalyst in oxidative degradation of metal complex dye has been investigated depending on the catalyst loading. The rate of the dye degradation increased with increasing catalyst dose from 0.5 to 1.0 g/L. When the GWTW concentration of 0.5 g/L was used, 27.5% of the SG dye decomposed during the first 10 min, whereas by doubling the amount of catalyst, the degradation efficiency increased up to 62.7% (Figure 10). After 60 min, about 85% and 67% of the dye color was removed with 1.0 and 0.5 g/L catalyst loading, respectively. The increased number of active sites on the surface of the GWTW catalyst can explain the enhancement of the SG dye degradation efficiency. The more active centers, the more the •OH radicals causing the destruction of the SG dye molecules can be formed.

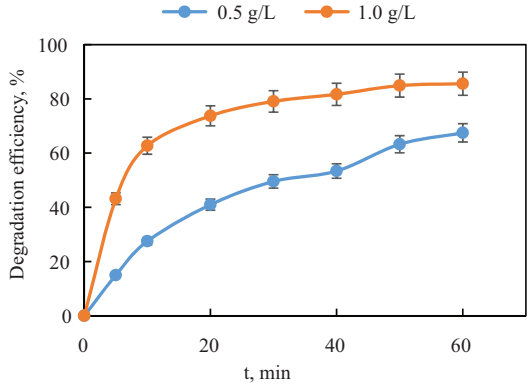

Figure 10. Effect of the catalyst loading on the SG dye degradation efficiency. Conditions: pH 3; C_0 (SG dye) = 100 mg/L; T = 50 °C

2.5. Effect of temperature on SG dye degradation efficiency

The effect of temperature on the SG dye solution decoloration was studied in the range of 20–60 °C, solution pH 3, and SG dye concentration 100 mg/L. After 10 min of reaction, the SG dye removal efficiencies were 27, 67, and 75% at 20, 50, and 60 °C, respectively. Faster degradation of SG dye with increasing temperature indicates not only increased mobility of the dye molecules but also an increased rate of catalytic reaction. The variation in temperature in the range of 293–323 K changed the rate of degradation of the SG dye because higher temperatures increased the rate of formation of •OH radicals in the reaction between H_2O_2 and GWTW (Xu et al., 2009; Wilkins, 1974). As we can see from the kinetic curves in Figure 11, the dye decoloration process can be divided into several kinetic regions (Benetoli et al., 2011): the first stage with a high reaction rate from the beginning of the reaction up to 10 min, the middle stage from 10 to 50 min after which equilibrium is approaching. Analysis of the experimental data of the first and second stages showed that they are in a good fit for the pseudo-first-order kinetics with high R^2 values (R^2 = 0.84–0.98). The catalytic degradation of organic dyes very often can be described by pseudo-first-order kinetics (Nasuha et al., 2021; Van et al., 2019).

As a significant excess of H_2O_2 was used in the SG dye degradation reaction, it can be considered as a pseudo-first-order with respect to the dye concentration (Deka et al., 2016):

$$\ln\left(\frac{C_t}{C_0}\right) \text{ or } \ln\left(\frac{A_t}{A_0}\right) = -kt, \tag{4}$$

where k is the degradation reaction apparent rate constant, C_0, C_t, A_0, and A_t are SG dye concentration and absorbance

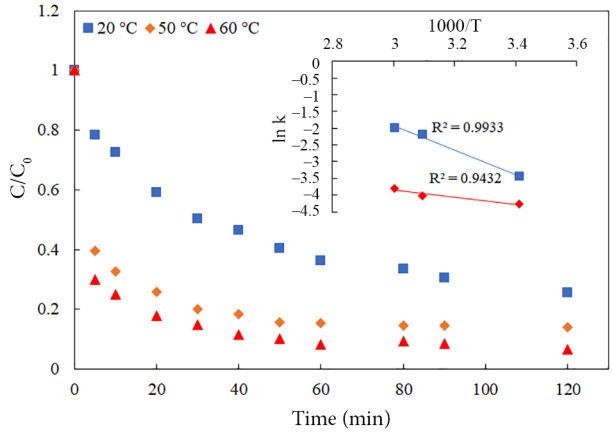

Figure 11. Effect of the reaction temperature on the kinetics of combined adsorption/catalytic degradation of SG dye. In the insert: Arrhenius plots for the first and second stages of reaction (from the data fitted to the pseudo-first-order kinetic model). Conditions: concentration of SG dye 100 mg/L, dye solution volume 10 mL, 1 mL H_2O_2, 5 mg GWTW catalyst, pH 3

Table 2. The rate constants and thermodynamic activation parameters for the first and second stages of the combined process of adsorption and catalytic oxidation of SG dye

Process stage	T, °C	The rate constant k, min^{-1}	E_a, kJ mol^{-1}	$\Delta H^{\#}$, kJ mol^{-1}	$\Delta S^{\#}$, kJ mol^{-1} K^{-1}	$\Delta G^{\#}$, kJ mol^{-1}
First	20	0.0322 (R^2 = 0.9179)	30.45	27.86	–0.178	80.01
(0–10 min)	50	0.1120 (R^2 = 0.8775)				85.35
Second (10–50 min)	60	0.1388 (R^2 = 0.8454)	8.65	6.07	–0.259	87.13
	20	0.0140 (R^2 = 0.9768)				81.96
	50	0.0181 (R^2 = 0.9739)				89.73
	60	0.0222 (R^2 = 0.9746)				92.32

before reaction and at time *t*. The values of apparent rate constant *k* were calculated at three temperatures from the slopes of the linear relationship $\ln(A_t/A_0) = f(t)$ and are listed in Table 2. The rate constants of catalytic oxidation of the SG dye with H_2O_2 and GWTW nanostructures are highly dependent on temperature increases. As the temperature rises from 20 °C to 60 °C in a Fenton-like system, the SG dye degradation reaction rate increased more than fourfold in the first stage and by a factor of 1.6 in the second (Table 2).

Activation energies E_a were determined from the slopes in the plots of linear dependence $\ln k = f(1/T)$ according to Eq. (5) (Deka et al., 2016):

$$\ln k = \ln A - E_a / RT, \quad (5)$$

where *k* is the degradation reaction rate constant, *A* is Arrhenius constant, E_a is activation energy (J mol^{-1}), *T* is the absolute temperature (K), and *R* is the universal gas constant (8.314472 J $K^{-1}mol^{-1}$).

The activation energy of the first stage of the SG dye degradation reaction is higher than that of the second stage and equals 30.45 kJ mol^{-1} (Table 2). Lin and Gurol (1998) studied the reaction of H_2O_2 with iron(III) oxide surface sites. The activation energy of H_2O_2 decomposition forming •OH radicals has been determined to be 32.8 kJ mol^{-1}.

The thermodynamic activation parameters of the SG dye catalytic degradation reaction were calculated using the linear form of the theoretical Eyring equation (Wilkins, 1974):

$$\ln\left(\frac{k}{T}\right) = \ln\left(\frac{K_B}{h}\right) - \frac{\Delta H^{\#}}{RT} + \frac{\Delta S^{\#}}{R}, \quad (6)$$

where *k* is the degradation reaction rate constant, *T* is the absolute temperature (K), K_B is Boltzmann's constant ($1.381 \cdot 10^{-23}$ J K^{-1}), *h* is Plank constant ($6.626 \cdot 10^{-34}$ J s), $\Delta H^{\#}$ is activation enthalpy (J mol^{-1}), $\Delta S^{\#}$ is activation entropy (J mol^{-1} K^{-1}), and *R* is the universal gas constant (8.314472 J $K^{-1}mol^{-1}$).

When using the linear plots of relationship $\ln(k/T) = f(1/T)$ (Eq. (6)), changes in activation enthalpy ($\Delta H^{\#}$) and entropy ($\Delta S^{\#}$) were resolved from the slopes and intercepts, respectively. The changes of free energy of activation ($\Delta G^{\#}$) were determined according to Eq. (7):

$$\Delta G^{\#} = \Delta H^{\#} - T\Delta S^{\#}. \quad (7)$$

The values of the $\Delta H^{\#}$, $\Delta S^{\#}$, and $\Delta G^{\#}$ for both stages of SG dye catalytic degradation reaction are presented in Table 2. The changes in activation enthalpy $\Delta H^{\#} > 0$ reflect the endothermic character of the SG dye degradation reaction under sunlight in the presence of H_2O_2 and GWTW. Meanwhile, the low negative value of $\Delta S^{\#}$ reflects a more ordered structure of transition state and a slight decrease in the dispersal of energy at the interface of active centers of GWTW and solution (Saha & Chowdhury, 2011). The values of changes of free energy of activation ($\Delta G^{\#}$) at three different temperatures range from 80.01 to 92.32 kJ mol^{-1}.

2.6. SG dye removal mechanism

Experimental results obtained using GWTW-SG dye adsorption systems have revealed the fact that dye removal is a strongly pH-dependent process. The effect of solution pH on SG dye removal efficiency is related to GWTW surface protonation degree. The negative molecules of the anionic SG dye are attracted by positively charged GWTW surface according to Eq. (8):

$$= FeOH_2^+ + A^- \rightarrow = FeA + H_2O. \quad (8)$$

In the case of heterogeneous catalytic SG dye degradation, the adsorption of both SG dye and H_2O_2 takes place on the GWTW surface (Figure 12). The formation of radicals from H_2O_2 at the surface of GWTW and the process of catalytic SG dye degradation could be explained based on several steps (Pinto et al., 2012). After addition to the GWTW-SG dye system, H_2O_2 molecules adsorb on the GWTW surface rich in Fe(III):

$$Fe_{surface}^{3+} + H_2O_2\ (aq) \rightarrow$$
$$[Fe_{surface}^{3+}H_2O_2(adsorbed)]. \quad (9)$$

Adsorbed H_2O_2 molecules reduce Fe(III) to Fe(II) forming Fe^{2+} and $O_2^{\bullet -}$ radicals:

$$[Fe_{surface}^{3+}H_2O_2(adsorbed)] \rightarrow$$
$$Fe_{surface}^{2+} + O_2^{\bullet -} + 2H^+. \quad (10)$$

Generated Fe^{2+} react with the adsorbed H_2O_2 forming very active •OH radicals (E = 2.38 V at pH 3.0):

$$Fe_{surface}^{2+}H_2O_2(adsorbed) \rightarrow$$
$$Fe_{surface}^{3+} + {\bullet}OH + {}^{-}OH. \quad (11)$$

•OH radicals attack and degrade SG dye molecules producing oxidation products:

$$\bullet OH + \text{SG dye} \rightarrow \text{oxidation products.} \quad (12)$$

It is known that dyes are cleaved when hydroxyl radicals react with organic molecules, mainly by removing hydrogen from the chemical bonds such as C-H, N-H, or O-H, or by adding hydrogen to the C = C bonds or the aromatic rings (Pignatello et al., 2006). However, decolored water can contain a lot of small organic matter (Collivignarelli et al., 2019), so in the future, we plan to study organic matter degradation and determine the COD and TOC parameters.

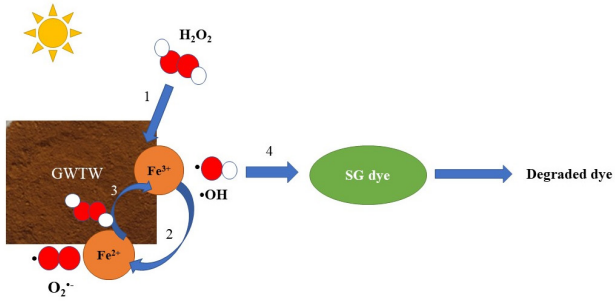

Figure 12. Scheme of the degradation of the SG dye using the heterogeneous Fenton-like catalyst prepared using sludge waste from groundwater treatment (GWTW)

2.7. Comparison of the SG dye removal using raw and calcined GWTW

It is well known that the studied material's physical properties and chemical composition influence its adsorption capacity and catalytic activity. For comparison, SG dye adsorption and catalytic degradation experiments were performed using untreated GWTW (W) and GWTW samples calcined at 800 °C (CW). As shown in Figure 13, the raw GWTW has a significantly higher potential to be used to remove SG dye from aqueous solutions compared to calcined samples. The SG dye removal by degradation (D) during the first 10 min is approximately four times higher in a system containing untreated GWTW (W). At 50 °C temperature, the removal efficiency is about 85% and 19% using untreated (W) and calcined (CW) samples of GWTW, respectively. The percentage of degraded SG dye at 50 °C temperature after 120 min of reaction increased up to 91% in the presence of W but only to 54% in the presence of CW. The adsorption capacity of the calcined material also decreased, but to a lesser extent compared to the decrease in catalytic activity in the SG dye degradation reaction. For both heterogeneous catalysts, untreated and calcined GWTW, higher degradation rates are observed at 50 °C temperature instead of lower 20 °C temperature (Figure 13). In contrast to degradation, the efficiency of SG dye removal by adsorption decreases with increasing temperature: only slightly with untreated GWTW, but by almost a third with calcined GWTW.

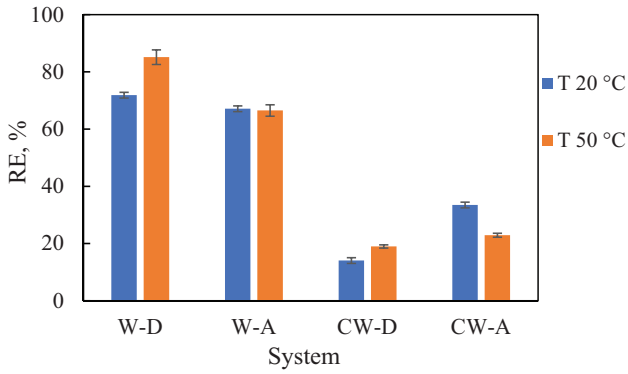

Figure 13. SG dye removal efficiency (RE) using raw (W) and calcined (CW) groundwater treatment waste (GWTW) for the dye degradation (D) or adsorption (A). Conditions: SG dye solution concentration 100 mg/L, the volume of dye solution 10 mL, 5 mg GWTW, 1 mL H_2O_2 for W-D and CW-D, pH 3, contact time 10 min

The different actions of untreated and pre-calcined GWTW could be explained by changes in the solid phase's chemical composition and structural properties during the calcination process. As mentioned above, XPS analysis showed that the major components of untreated GWTW are hydrous ferric oxide, α-Fe_2O_3 (hematite), and Fe(OH)O (goethite, lepidocrocite). While, according to the XRD analysis, the main phase of the calcined sample containing iron was maghemite (γ-Fe_2O_3). Calcination of GWTW not only involves the transformation of iron(III) phases and a change in GWTW color (from brown to red), but also the remaining constituents can be converted to another form or removed at all. These changes may affect the catalytic activity of GWTW. Besides, the specific surface area of the amorphous GWTW is relatively higher when compared to its crystalline form leading to a higher adsorption capacity. The catalytic efficiency of the material is related to its adsorption ability (Xiao et al., 2018; Pinto et al., 2012). The larger the area of the GWTW, the richer it is in the number of active centers suitable for the interaction between the catalyst, H_2O_2, and the dye molecules.

The GWTW catalyst is suitable for reuse in the Fenton process because the weight loss of GWTW after one cycle is less than 0.2%. Besides, the catalyst particles do not agglomerate after separation, so that GWTW can be reused with another portion of the dye solution and peroxide.

2.8. Comparison of adsorption and catalytic properties of materials used for the dye removal

The adsorbents of various types were tested for the adsorptive removal of metal complex anionic dye Sanodure Green (Figure 14). Batch experiments were carried out with the aim to compare the dye removal rate and removal capacity using different adsorbents. As can be seen from Figure 14, the adsorptive properties of GWTW are comparable with those of the powdered activated carbon. More than 96% and 88% of the dye color can be removed in the first 3 min with the aid of GWTW, and Norit PK 1-3 activated carbon, respectively.

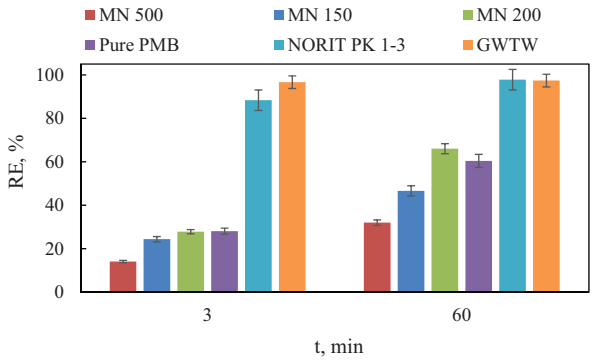

Figure 14. Comparison of SG dye adsorption capacity in various adsorbents. Conditions: SG dye solution pH 2, adsorbent dose 4 g/L, temperature 20 °C

When polymeric materials (macroporous resins MN 500, MN 150, MN 200, and mixed bed resin PMB) are used as adsorbents, only 14–28% of the color of the dye solution can be removed at the same time. Over time, their adsorption capacities toward SG dye increase, but even after 60 min, they do not equal the adsorption capacities of GWTW and activated carbon. In addition, the advantage of the GWTW is that it can be used both as an adsorbent and as a catalyst. The catalytic activity of GWTW in the Fenton-like reaction was evaluated considering the data presented in the literature (Table 3). Despite the difference in the operating parameters and the variety of the studied dyes, we can see that the degradation efficiencies of GWTW and the other iron-rich compounds are at a similar level. The advantage of the catalyst used in this study is that specific preparation is not required. Although the initial concentration of the SG dye solution was relatively high and reached 100 mg/L, 92% degradation was achieved within 50 min (Table 3).

Table 3. Comparison of catalytic activity of the GWTW with the other Fe(III) containing catalysts reported in the literature (COD – chemical oxygen demand; RE – removal efficiency)

Reference	Pollutant	Catalyst	Optimum conditions and operating parameters	Results
Huang et al., 2011	Dispersed Orange 288	Nano-iron oxides/ goldmine waste-solid	3.0 g catalyst waste-solid, 100 mL of dye solution, 5 mL of H_2O_2, Temperature 30 °C, pH < 1, Time 2 h	COD removal efficiency 68.6%
Guz et al., 2014	Crystal Violet (CV)	Iron modified montmorillo-nite (MMT-Fe)	1.5 g/L MMT-Fe, 100 mL 0.060 mM CV, 30% H_2O_2, Temperature 25 °C, Time 2 h, 300 W solar lamp	RE 99.9%
Zheng et al., 2015	Congo Red (CR), Eosin Red (ER), Methylene Blue (MB)	α-Fe_2O_3	0.2 g α-Fe_2O_3, 200 mL dye solutions (10 mg/L), Room temperature, Time 50 min, Visible light irradiation	RE of MB (57%) < ER (63%) < CR (93%)
Xiao et al., 2018	Acid Red G	α-Fe_2O_3	0.1 g α-Fe_2O_3, 0.1 L 50 mg/L dye, 0.3 mL of H_2O_2 solution (30 wt%), pH 2, Time 90 min, LED lamp (λ = 420 nm) irradiation	RE 98%
Rubeena et al., 2018	Acid Red 1 (AR1)	Iron loaded rice husk biochar (Fe-RHB) and coir pith biochar (Fe-CPB)	5 g/L and 4 g/L for Fe-RHB and Fe-CPB, respectively, 200 mL dye (50 mg/L), 16 mM H_2O_2, The temperature 30 °C, pH 3, Time 120 min	RE 97.6% (Fe-RHB) and 99.1% (Fe-CPB)
Domacena et al., 2020	Methyl Orange (MO)	α-Fe_2O_3 powders	30 mg α-Fe_2O_3 powders, 30 ml 2.5 ppm MO, 30 μL H_2O_2, Time 2 h, UVC lamp 10×2 W, 2.5 ppm	RE 76.5%

End of Table 3

Reference	Pollutant	Catalyst	Optimum conditions and operating parameters	Results
Nadeem et al., 2020	Synozol Red	$ZnFe_2O_4$ and graphene oxide based $ZnFe_2O_4$ composite	75 mg/L for $ZnFe_2O_4$ and 50 mg/L for GO-$ZnFe_2O_4$, H_2O_2 dose = 27 mM, pH = 3, Irradiation time = 60 min	RE 57% and 94%
Xu et al., 2021	Methylene Blue (MB)	α-Fe_2O_{3-x}	10 mg α-Fe_2O_{3-x}, 50 mL of MB aqueous solution (0.02 mM), 255 µL of H_2O_2 solution (30 wt%), Room temperature, pH 2.0, Time 40 min, 300 W xenon lamp	RE 82%
Nasuha et al., 2021	Methylene Blue (MB), Acid Blue 29 (AB29)	Slag activated by sulfuric acid (S-EAF)	S-EAF dosage 0.04 g (AB29) and 0.02 g (MB), C_0 (dye) = 50 mg/L, 6 mM (AB29) and 8 mM (MB) H_2O_2 concentration, Temperature 30 °C, pH = 4.5	RE 95% and 82%
This study	Sanodure Green LWN	Groundwater treatment waste (GWTW)	5 mg GWTW catalyst, 10 mL SG dye (100 mg/L), 1 mL H_2O_2 (30 wt%), Temperature 50 °C, pH 3, Time 50 min	RE 92%

Conclusions

Groundwater treatment waste (GWTW) has been successfully utilized for the decoloration of the metal complex dye Sanodure green LWN solutions due to its unique natural properties. The raw GWTW was more suitable for dye removal than calcined at 800 °C temperature. The high decoloration rate (up to 70 % in the first 5 min) was achieved by a combined adsorption/degradation process using GWTW as adsorbent and catalyst, H_2O_2 as oxidant, and natural sunlight as an energy source. Adsorption or non-catalytic peroxidation alone was less effective in removing SG dye. The acidic medium (pH 2–3) was more favorable not only for the adsorption but also for the degradation of SG dye. The solution decoloration rate increased with an increase in temperature. The process of SG dye catalytic degradation can be divided into several kinetic regions with different rate constants and activation energy values. The dye degradation reaction is endothermic in nature and is controlled by the enthalpy of activation.

This study concludes that the usage of GWTW could be considered a sustainable way for the pre-treatment of dye-contaminated wastewater before it enters the wastewater treatment plant.

References

Albrektienė, R., Karaliūnas, K., & Bazienė, K. (2019). Sustainable reuse of groundwater treatment iron sludge for organic matter removal from river Neris water. *Sustainability*, *11*(3), 639–654. https://doi.org/10.3390/su11030639

Ali, M. E. M., Gad-Allah, T. A., & Badawy, M. I. (2013). Heterogeneous Fenton process using steel industry wastes for methyl orange degradation. *Applied Water Science*, *3*, 263–270. https://doi.org/10.1007/s13201-013-0078-1

Aragaw, T. A., Bogale, F. M., & Aragaw, B. A. (2021). Iron-based nanoparticles in wastewater treatment: A review on synthesis methods, applications, and removal mechanisms. *Journal of Saudi Chemical Society*, *25*(8), 101280. https://doi.org/10.1016/j.jscs.2021.101280

Arora, C., Kumar, P., Soni, S., Mittal, J., Mittal, A., & Singh, B. (2020). Efficient removal of malachite green dye from aqueous solution using *Curcuma caesia* based activated carbon. *Desalination and Water Treatment Science and Engineering*, *195*, 341–352. https://doi.org/10.5004/dwt.2020.25897

Azha, S. F., Shahadat, M., Ismail, S., Ali, S. W., & Ahammad, S. Z. (2021). Prospect of clay-based flexible adsorbent coatings as cleaner production technique in wastewater treatment, challenges, and issues: A review. *Journal of the Taiwan Institute of Chemical Engineers, 120*, 178–206. https://doi.org/10.1016/j.jtice.2021.03.018

Babatunde, A. O., & Zhao, Y. O. (2007). Constructive approaches toward water treatment works sludge management: An international review of beneficial reuses. *Critical Reviews in Environmental Science and Technology*, *37*(2), 129–164. https://doi.org/10.1080/10643380600776239

Banazadeh, A., Salimi, H., Khaleghi, M., & Shafiei-Haghighi, S. (2016). Highly efficient degradation of hazardous dyes in aqueous phase by supported palladium nanocatalyst–a green approach. *Journal of Environmental Chemical Engineering*, *4*(2), 2178–2182. https://doi.org/10.1016/j.jece.2015.09.007

Bartošová, A., Blinová, L., Sirotiak, M., & Michalíková, A. (2017). Usage of FTIR-ATR as non-destructive analysis of selected toxic dyes. *Research Papers Faculty of Materials Science and Technology Slovak University of Technology*, *25*(40), 103–111. https://doi.org/10.1515/rput-2017-0012

Bello, M. M., & Raman, A. A. A. (2019). Synergy of adsorption and advanced oxidation processes in recalcitrant wastewater

treatment. *Environmental Chemistry Letters*, *17*, 1125–1142. https://doi.org/10.1007/s10311-018-00842-0

Benetoli, L. O. de B., Cadorin, B. M., Postiglione, C. da S., de Souza, I. G., & Debacher, N. A. (2011). Effect of temperature on methylene blue decolorization in aqueous medium in electrical discharge plasma reactor. *Journal of Brazilian Chemical Society, 22*(9), 1669–1678. https://doi.org/10.1590/S0103-50532011000900008

Bhat, A. P., & Gogate, P. R. (2021). Degradation of nitrogen-containing hazardous compounds using advanced oxidation processes: A review on aliphatic and aromatic amines, dyes, and pesticides. *Journal of Hazardous Materials*, *403*, 123657. https://doi.org/10.1016/j.jhazmat.2020.123657

Bokare, A. D., & Choi, W. (2014). Review of iron-free Fenton-like systems for activating H_2O_2 in advanced oxidation processes. *Journal of Hazardous Materials*, *275*, 121–135. https://doi.org/10.1016/j.jhazmat.2014.04.054

Chang, Ch.-Ch., Chiang, F.-Ch., Chen, Sh.-M., Thangavelu, K., & Yang, H.-J. (2016). Studies on electrochemical oxidation of aluminum and dyeing in various additives towards industrial applications. *International Journal of Electrochemical Science*, *11*, 2142–2150.

Clariant. (2014). *Aluminum finishing. Specific color solutions*. Clariant International Ltd.

Clariant. (2020). *Sanodure Green LWN safety data sheet*. https://www.clariant.com/en/Solutions/Products/2014/03/18/17/07/Sanodure-Green-LWN

Collivignarelli, M. C., Abb, A., Miino, M. C., & Damiani, S. (2019). Treatments for color removal from wastewater: State of the art. *Journal of Environmental Management*, *236*, 727–745. https://doi.org/10.1016/j.jenvman.2018.11.094

Deka, P., Hazarika, A., Deka, R. C., & Bharali, P. (2016). Influence of CuO morphology on the enhanced catalytic degradation on methylene blue and methyl orange. *RSC Advances*, *6*, 95292–95305. https://doi.org/10.1039/C6RA20173C

Diliūnas, J., Jurevičius, A., & Zuzevičius, A. (2006). Formation of iron compounds in the Quaternary groundwater of Lithuania. *Geologija*, *55*, 66–73.

Domacena, A. M. G., Aquino, C. L. E., & Balela, M. D. L. (2020). Photo-Fenton degradation of methyl orange using hematite (α-Fe_2O_3) of various morphologies. *Materials Today: Proceedings*, *22*, 248–254. https://doi.org/10.1016/j.matpr.2019.08.095

Dzombak, D. A., & Morel, F. M. M. (1990). *Surface complexation modeling: Hydrous Ferric Oxide*. John Wiley & Sons.

Garrido-Ramírez, E. G., Theng, B. K. G., & Mora, M. L. (2010). Clays and oxide minerals as catalysts and nanocatalysts in Fenton-like reactions – A review. *Applied Clay Science*, *47*(3–4), 182–192. https://doi.org/10.1016/j.clay.2009.11.044

Grosvenor, A. P., Kobe, B. A., Biesinger, M. C., & McIntyre, N. S. (2004). Investigation of multiplet splitting of Fe 2p XPS spectra and bonding in iron compounds. *Surface and Interface Analysis*, *36*(12), 1564–1574. https://doi.org/10.1002/sia.1984

Gupta, V. K., Agarwal, S., Ahmad, R., Mirza, A., & Mittal, J. (2020). Sequestration of toxic congo red dye from aqueous solution using ecofriendly guar gum/activated carbon nanocomposite. *International Journal of Biological Macromolecules*, *158*, 1310–1318. https://doi.org/10.1016/j.ijbiomac.2020.05.025

Guz, L., Curutchet, G., Torres Sánchez, R. M., & Candal, R. (2014). Adsorption of crystal violet on montmorillonite (or iron modified montmorillonite) followed by degradation through Fenton or photo-Fenton type reactions. *Journal of Environmental Chemical Engineering*, *2*(4), 2344–2351. https://doi.org/10.1016/j.jece.2014.02.007

Haddad, B., Mittal, A., Mittal, J., Paolone, A., Villemin, D., Debdab, M., Mimanne, G., Habibi, A., Hamidi, Z., Boumediene, M., & Belarbi, E.-h. (2021). Synthesis and characterization of Egg shell (ES) and Egg shell with membrane (ESM) modified by ionic liquids. *Chemical Data Collections*, *33*, 100717. https://doi.org/10.1016/j.cdc.2021.100717

Heber, T. (2015). *Weather fast adsorptive dyeing of anodized aluminum for outdoor applications* [Conference presentation]. 2015 Anodizing Conference, San Diego, California.

Horáková, M., Klementová, Š., Kříž, P., Balakrishna, S. K., Špatenka, P., Golovko, O., Hájková, P., & Exnar, P. (2014). The synergistic effect of advanced oxidation processes to eliminate resistant chemical compounds. *Surface and Coatings Technology*, *241*, 154–158. https://doi.org/10.1016/j.surfcoat.2013.10.068

Hou, P., Shi, C., Wu, L., & Hou, X. (2016). Chitosan/hydroxyapatite/Fe_3O_4 magnetic composite for metal-complex dye AY220 removal: Recyclable metal-promoted Fenton-like degradation. *Microchemical Journal*, *128*, 218–225. https://doi.org/10.1016/j.microc.2016.04.022

Huang, M., Zhao, K., Zhang, M., Chen, Sh., Xu, W., Ye, Y., Fu, W., Wei, Y., Qiu, Z., & Sun, F. (2011). Removal of disperse dyes from wastewater by nano-iron modified goldmine waste-solid assisted AOPs. *Procedia Engineering*, *18*, 358–362. https://doi.org/10.1016/j.proeng.2011.11.057

Jabeen, A., & Bhatti, H. N. (2021). Adsorptive removal of reactive green 5 (RG-5) and direct yellow 50 (DY-50) from simulated wastewater by *Mangifera indica* seed shell and its magnetic composite: Batch and Column study. *Environmental Technology & Innovation*, *23*, 101685. https://doi.org/10.1016/j.eti.2021.101685

Kan, T., Strezov, V., Evans, T., & Nelson, P. (2016). Analysis of water produced during thermal decomposition of goethitic iron ore. *International Journal of Chemical Engineering and Applications*, *7*(5), 327–330. https://doi.org/10.18178/ijcea.2016.7.5.599

Katsoukis, G., Jun Jo, W., & Frei, H. (2019). Structure and orientation of molecular wires embedded in ultrathin silica membrane for artificial photosynthesis elucidated by polarized FT-IRRAS. *Journal of Physical Chemistry C*, *123*(31), 18905–18913. https://doi.org/10.1021/acs.jpcc.9b02523

Kausar, A., Naeem, K., Iqbal, M., Nazli, Z.-H., Bhatti, H. N., Ashraf, A., Nazir, A., Kusuma, H. S., & Khan, M. I. (2021). Kinetics, equilibrium and thermodynamics of dyes adsorption onto modified chitosan: A review. *Zeitschrift für Physikalische Chemie*. https://doi.org/10.1515/zpc-2019-1586

Lai, C., Shi, X., Li, L., Cheng, M., Liu, X., Liu, S., Li, B., Yi, H., Qin, L., Zhang, M., & An, N. (2021). Enhancing iron redox cycling for promoting heterogeneous Fenton performance: A review. *Science of the Total Environment*, *775*, 145850. https://doi.org/10.1016/j.scitotenv.2021.145850

Leiviskä, T., Leskelä, T., & Tanskanen, J. (2019). Effect of alkali regeneration on pore characteristics and performance of ferric oxyhydroxide and akaganéite sorbents. *Journal of Water Process Engineering*, *31*, 100838. https://doi.org/10.1016/j.jwpe.2019.100838

Li, X., Xiao, B., Wu, M., Wang, L., Chen, R., Wei, Y., & Liu, H. (2020). In-situ generation of multi-homogeneous/heterogeneous Fe-based Fenton catalysts toward rapid degradation of organic pollutants at near neutral pH. *Chemosphere*, *245*, 125663. https://doi.org/10.1016/j.chemosphere.2019.125663

Li, Y., & Zhang, F.-S. (2010) Catalytic oxidation of Methyl Orange by an amorphous FeOOH catalyst developed from a high iron-containing fly ash. *Chemical Engineering Journal*, *158*(2), 148–153. https://doi.org/10.1016/j.cej.2009.12.021

Lin, S.-S., & Gurol, M. D. (1998). Catalytic decomposition of hydrogen peroxide on iron oxide: Kinetics, mechanism, and implications. *Environmental Science and Technology*, *32*(10), 1417–1423. https://doi.org/10.1021/es970648k

Luo, H., Zeng, Y., He, D., & Pan, X. (2021). Application of iron-based materials in heterogeneous advanced oxidation processes for wastewater treatment: A review. *Chemical Engineering Journal*, *407*, 127191. https://doi.org/10.1016/j.cej.2020.127191

Mariyam, A., Mittal, J., Sakina, F., Baker, R. T., & Sharma, A. K. (2021a). Adsorption behaviour of Chrysoidine R dye on a metal/halide-free variant of ordered mesoporous carbon. *Desalination and Water Treatment Science and Engineering*, *223*, 425–433. https://doi.org/10.5004/dwt.2021.27147

Mariyam, A., Mittal, J., Sakina, F., Baker, R. T., Sharma, A. K., & Mittal, A. (2021b). Efficient batch and Fixed-Bed sequestration of a basic dye using a novel variant of ordered mesoporous carbon as adsorbent. *Arabian Journal of Chemistry, 14*(6), 103186. https://doi.org/10.1016/j.arabjc.2021.103186

McIntyre, N. S., & Zetaruk, G. (1977). X-ray photoelectron spectroscopic studies of iron oxides. *Analytical Chemistry*, *49*(11), 1521–1529. https://doi.org/10.1021/ac50019a016

Miao, X., Dai, H., Chen, J., & Zhu, J. (2018). The enhanced method of hydroxyl radical generation in the heterogeneous UV-Fenton system with α-FeOOH as catalyst. *Separation and Purification Technology*, *200*, 36–43. https://doi.org/10.1016/j.seppur.2018.02.012

Mittal, A., & Mittal, J. (2015). Hen feather: A remarkable adsorbent for dye removal. In S. K. Sharma (Ed.), *Green chemistry for dyes removal from wastewater: Research trends and applications* (pp. 409–457). Scrivener Publishing LLC. https://doi.org/10.1002/9781118721001.ch11

Mittal, J. (2020). Permissible synthetic food dyes in India. *Resonance, 25*, 567–577. https://doi.org/10.1007/s12045-020-0970-6

Montoya-Bautista, C. V., Avella, E., Ramírez-Zamora, R.-M., & Schouwenaars, R. (2019). Metallurgical wastes employed as catalysts and photocatalysts for water treatment: A review. *Sustainability*, *11*(9), 2470–2486. https://doi.org/10.3390/su11092470

Moradi, M., Elahinia, A., Vasseghian, Y., Dragoi, E.-N., Omidi, F., & Khaneghah, A. M. (2020). A review on pollutants removal by Sono-photo -Fenton processes. *Journal of Environmental Chemical Engineering*, *8*(5), 104330. https://doi.org/10.1016/j.jece.2020.104330

Nadeem, N., Zahid, M., Tabasum, A., Mansha, A., Jilani, A., Bhatti, I. A., & Bhatti, H. N. (2020). Degradation of reactive dye using heterogeneous photo-Fenton catalysts: Zn-Fe_2O_4 *and GO*-$ZnFe_2O_4$ composite. *Materials Research Express*, *7*(1), 015519. https://doi.org/10.1088/2053-1591/ab66ee

Nasuha, N., Hameed, B. H., & Okoye, P. U. (2021). Dark-Fenton oxidative degradation of methylene blue and acid blue 29 dyes using sulfuric acid-activated slag of the steel-making process. *Journal of Environmental Chemical Engineering*, *9*(1), 104831. https://doi.org/10.1016/j.jece.2020.104831

Neyens, E., & Baeyens, J. (2003). A review of classic Fenton's peroxidation as an advanced oxidation technique. *Journal of Hazardous Materials*, *98*(1–3), 33–50. https://doi.org/10.1016/S0304-3894(02)00282-0

Nguyen, T. T., Huynh, K. A., Padungthon, S., Pranudta, A., Amonpattaratkit, P., Tran, L. B., Phan, P. T., & Nguyen, N. H. (2021). Synthesis of natural flowerlike iron-alum oxide with special interaction of Fe-Si-Al oxides as an effective catalyst for heterogeneous Fenton process. *Journal of Environmental Chemical Engineering*, *9*(4), 105732. https://doi.org/10.1016/j.jece.2021.105732

Noreen, S., Bhatti, H. N., Iqbal, M., Hussain, F., & Sarim, F. M. (2020). Chitosan, starch, polyaniline and polypyrrole biocomposite with sugarcane bagasse for the efficient removal of Acid Black dye. *International Journal of Biological Macromolecules*, *147*, 439–452. https://doi.org/10.1016/j.ijbiomac.2019.12.257

Novoselova, L. Y. (2013). Composition, structure and sorbability of the thermally treated water deironing precipitate with respect to carbon monoxide. *Powder Technology*, *243*, 149–153. https://doi.org/10.1016/j.powtec.2013.03.032

Ociński, D., Jacukowicz-Sobala, I., Mazur, P., Raczyk, J., & Kociołek-Balawejder, E. (2016). Water treatment residuals containing iron and manganese oxides for arsenic removal from water – Characterization of physicochemical properties and adsorption studies. *Chemical Engineering Journal*, *294*, 210–221. https://doi.org/10.1016/j.cej.2016.02.111

Oliveira, C., Santosa, M. S. F., Maldonado-Hódar, F. J., Schaule, G., Alves, A., & Madeira, L. M. (2012). Use of pipe deposits from water networks as novel catalysts in paraquat peroxidation. *Chemical Engineering Journal*, *210*, 339–349. https://doi.org/10.1016/j.cej.2012.09.001

Oller, I., Malato, S., & Sanchez-Perez, J. A. (2011). Combination of advanced oxidation processes and biological treatments for wastewater decontamination – A review. *Science of Total Environment*, *409*(20), 4141–4166. https://doi.org/10.1016/j.scitotenv.2010.08.061

Ong, D. C., Kan, C. Ch., Mae, Sh., Pingul-Ong, B., & de Luna, M. D. G. (2017). Utilization of groundwater treatment plant (GWTP) sludge for nickel removal from aqueous solutions: Isotherm and kinetic studies. *Journal of Environmental Chemical Engineering*, *5*(6), 5746–5753. https://doi.org/10.1016/j.jece.2017.10.046

Pal, S., Singh, P. N., Verma, A., Kumar, A., Tiwary, D., Prakash, R., & Sinha, I. (2020). Visible light photo-Fenton catalytic properties of starch functionalized iron oxyhydroxide nanocomposites. *Environmental Nanotechnology, Monitoring & Management*, *14*, 100311. https://doi.org/10.1016/j.enmm.2020.100311

Paredes-Laverde, M., Salamanca, M., Diaz-Corrales, J. D., Flórez, E., Silva-Agredo, J., & Torres-Palma, R. A. (2021). Understanding the removal of an anionic dye in textile wastewaters by adsorption on $ZnCl_2$ activated carbons from rice and coffee husk wastes: A combined experimental and theoretical study. *Journal of Environmental Chemical Engineering*, *9*(4), 105685. https://doi.org/10.1016/j.jece.2021.105685

Patel, A., Soni, S., Mittal, J., Mittal, A., & Arora, C. (2021). Sequestration of crystal violet from aqueous solution using ash of black turmeric rhizome. *Desalination and Water Treatment*, *220*, 342–352. https://doi.org/10.5004/dwt.2021.26911

Prati, S., Milosevic, M., Sciutto, G., Bonacini, I., Kazarian, S. G., & Mazzeo, R. (2016). Analyses of trace amounts of dyes with a new enhanced sensitivity FTIR spectroscopic technique: MU-ATR (metal underlayer ATR spectroscopy). *Analytica Chimica Acta*, *941*, 67–79. https://doi.org/10.1016/j.aca.2016.09.005

Perrotti, T. C., Freitas, N. S., Alzamora, M., Sánchez, D. R., & Carvalho, N. M. F. (2019). Green iron nanoparticles supported on amino-functionalized silica for removal of the dye methyl orange. *Journal of Environmental Chemical Engineering*, *7*(4), 103237. https://doi.org/10.1016/j.jece.2019.103237

Pignatello, J. J., Oliveros, E., & Mackay, A. (2006). Advanced oxidation processes for organic contaminant destruction based on the Fenton reaction and related chemistry. *Critical Reviews in Environmental Science and Technology*, *36*(1), 1–84. https://doi.org/10.1080/10643380500326564

Pinto, I. S. X., Pacheco, P. H. V. V., Coelho, J. V., Lorençon, E., Ardisson, J. D., Fabris, J. D., de Souza, P. P., Krambrock, K. W. H., Oliveira, L. C. A., & Pereira, M. C. (2012). Nanostructured δ-FeOOH: An efficient Fenton-like catalyst for the oxidation of organics in water. *Applied Catalysis B: Environmental*, *119–120*, 175–182. https://doi.org/10.1016/j.apcatb.2012.02.026

Prucek, R., Hermanek, M., & Zbořil, R. (2009). An effect of iron(III) oxides crystallinity on their catalytic efficiency and applicability in phenol degradation – A competition between homogeneous and heterogeneous catalysis. *Applied Catalysis A: General*, *366*(2), 325–332. https://doi.org/10.1016/j.apcata.2009.07.019

Rubeena, K. K., Prasad Reddy, P. H., Laiju, A. R., & Nidheesh, P. V. (2018). Iron impregnated biochars as heterogeneous Fenton catalyst for the degradation of acid red 1 dye. *Journal of Environmental Management*, *226*, 320–328. https://doi.org/10.1016/j.jenvman.2018.08.055

Saha, P., & Chowdhury, Sh. (2011). Insight into adsorption thermodynamics. In M. Tadashi (Ed.), *Thermodynamics, CC-BY-NC-SA* (pp. 349–364). InTech. https://doi.org/10.5772/13474

Saharan, S., Kumar, V., Mittal, J., Sharma, V., & Sharma, A. K. (2021). Efficient ultrasonic assisted adsorption of organic pollutants employing bimetallic-carbon nanocomposites. *Separation Science and Technology*, *56*(17), 2895–2908. https://doi.org/10.1080/01496395.2020.1866608

Sanchis, R., Dejoz, A., Vázquez, I., Vilarrasa-García, E., Jiménez-Jiménez J., Rodríguez-Castellón, E., Nieto, J. M. L., & Solsona, B. (2019). Ferric sludge derived from the process of water purification as an efficient catalyst and/or support for the removal of volatile organic compounds. *Chemosphere*, *219*, 286–295. https://doi.org/10.1016/j.chemosphere.2018.12.002

Santos, V. P., Pereira, M. F. R., Faria, P. C. C., & Órfão, J. J. M. (2009). Decolourisation of dye solutions by oxidation with H_2O_2 in the presence of modified activated carbons. *Journal of Hazardous Materials*, *162*(2–3), 736–742. https://doi.org/10.1016/j.jhazmat.2008.05.090

Siswoyo, E., Mihara, Y., & Tanaka, Sh. (2014). Determination of key components and adsorption capacity of a low cost adsorbent based on sludge of drinking water treatment plant to adsorb cadmium ion in water. *Applied Clay Science*, *97–98*, 146–150. https://doi.org/10.1016/j.clay.2014.05.024

Sodaitienė, E., Gefenienė, A., Kaušpėdienė, D., Ragauskas, R., Vaičiūnienė, J., Selskienė, A., Jasulaitienė, V., & Ramanauskas, R. (2021). Sustainable removal of anodized aluminum dye by groundwater treatment waste: Experimental and modeling. *Heliyon*, *7*(1), e05993. https://doi.org/10.1016/j.heliyon.2021.e05993

Soni, S., Bajpai, P. K., Bharti, D., Mittal, J., & Arora, C. (2020). Removal of crystal violet from aqueous solution using iron based metal organic framework. *Desalination and Water Treatment Science and Engineering*, *205*, 386–399. https://doi.org/10.5004/dwt.2020.26387

Sun, Y., Gu, Y., & Zha, Q. (2021). A novel surface imprinted resin for the selective removal of metal-complexed dyes from aqueous solution in batch experiments: ACB GGN as a representative contaminant. *Chemosphere*, *280*, 130611. https://doi.org/10.1016/j.chemosphere.2021.130611

Tang, Y., Li, M., Mu, C., Zhou, J., & Shi, B. (2019). Ultrafast and efficient removal of anionic dyes from wastewater by polyethyleneimine-modified silica nanoparticles. *Chemosphere, 229*, 570–579. https://doi.org/10.1016/j.chemosphere.2019.05.062

Thomas, N., Dionysiou, D. D., & Pillai, S. C. (2021). Heterogeneous Fenton catalysts: A review of recent advances. *Journal of Hazardous Materials*, *404*(B), 124082. https://doi.org/10.1016/j.jhazmat.2020.124082

Van, H. T., Nguyen, L. H., Hoang, T. K., Tran, T. P., Vo, A. T., Pham, T. T., & Nguyen, X. C. (2019). Using FeO-constituted iron slag wastes as heterogeneous catalyst for Fenton and ozonation processes to degrade *Reactive Red 24* from aqueous solution. *Separation and Purification Technology*, *224*, 431–442. https://doi.org/10.1016/j.seppur.2019.05.048

Wilkins, R. C. (1974). *The study of the kinetics and mechanism of reactions of transition metal complexes.* Allyn and Bacon.

Wołowiec, M., Pruss, M., Komorowska-Kaufman, A., Lasocka Gomuła, I., Rzepa, G., & Bajda, T. (2019). The properties of sludge formed as a result of coagulation of backwash water from filters removing iron and manganese from groundwater. *SN Applied Sciences*, *1*, 639. https://doi.org/10.1007/s42452-019-0653-7

Xiao, C., Jun Li, J., & Zhang, G. (2018). Synthesis of stable burger-like α-Fe_2O_3 catalysts: Formation mechanism and excellent photo-Fenton catalytic performance. *Journal of Cleaner Production*, *180*, 550–559. https://doi.org/10.1016/j.jclepro.2018.01.127

Xu, H.-Y., Prasad, M., & Liu, Y. (2009). Schorl: a novel catalyst in mineral-catalyzed Fenton-like system for dyeing wastewater discoloration. *Journal of Hazardous Materials*, *165*(1–3), 1186–1192. https://doi.org/10.1016/j.jhazmat.2008.10.108

Xu, W., Xue, W., Huang, H., Wang, J., Zhong, C., & Mei, D. (2021). Morphology controlled synthesis of α-Fe_2O_{3-x} with benzimidazole-modified Fe-MOFs for enhanced photo-Fenton-like catalysis. *Applied Catalysis B: Environmental*, *291*, 120129. https://doi.org/10.1016/j.apcatb.2021.120129

Yao, Y., Wang, L., Sun, L., Zhu, S., Huang, Z., Mao, Y., Lu, W., & Chen, W. (2013). Efficient removal of dyes using heterogeneous Fenton catalysts based on activated carbon fibers with enhanced activity. *Chemical Engineering Science*, *101*, 424. https://doi.org/10.1016/j.ces.2013.06.009

Zhang, T., Zhao, N., Li, J., Gong, H., An, T., Zhao, F., & Ma, H. (2017). Thermal behavior of nitrocellulose-based superthermites: Effects of nano-Fe_2O_3 with three morphologies. *RSC Advances*, *7*(38), 23583. https://doi.org/10.1039/C6RA28502C

Zheng, X., Jiao, Y., Chai, F., Qu, F., Umar, A., & Wu, X. (2015). Template-free growth of well-crystalline α-Fe_2O_3 nanopeanuts with enhanced visible-light driven photocatalytic properties. *Journal of Colloid and Interface Science*, *457*, 345–352. https://doi.org/10.1016/j.jcis.2015.07.023

Zhu, Y., Zhu, R., Xi, Y., Zhu, J., Zhu, G., & He, H. (2019). Strategies for enhancing the heterogeneous Fenton catalytic reactivity: A review. *Applied Catalysis B: Environmental*, *255*, 117739. https://doi.org/10.1016/j.apcatb.2019.05.041

Zubrytė, E., Gefenienė, A., Kaušpėdienė, D., Ragauskas, R., Binkienė, R., Selskienė, A., & Pakštas, V. (2020). Fast removal of Pb(II) and Cu(II) from contaminated water by groundwater treatment waste: Impact of sorbent composition. *Separation Science and Technology*, *55*(16), 2855–2868. https://doi.org/10.1080/01496395.2019.1655455